

# Supervising Embedding Algorithms Using the Stress

Ery Arias-Castro \*

Phong Alain †

## Abstract

While classical scaling, just like principal component analysis, is parameter-free, most other methods for embedding multivariate data require the selection of one or several parameters. This tuning can be difficult due to the unsupervised nature of the situation. We propose a simple, almost obvious, approach to supervise the choice of tuning parameter(s): minimize a notion of stress. We substantiate this choice by reference to rigidity theory. We extend a result by Aspnes et al. (*IEEE Mobile Computing*, 2006), showing that general random geometric graphs are trilateration graphs with high probability. And we provide a stability result à la Anderson et al. (*SIAM Discrete Mathematics*, 2010). We illustrate this approach in the context of the MDS-MAP(P) algorithm of Shang and Ruml (*IEEE INFOCOM*, 2004). As a prototypical patch-stitching method, it requires the choice of patch size, and we use the stress to make that choice data-driven. In this context, we perform a number of experiments to illustrate the validity of using the stress as the basis for tuning parameter selection. In so doing, we uncover a bias-variance tradeoff — a phenomenon which may have been overlooked in the multidimensional scaling literature. By turning MDS-MAP(P) into a method for manifold learning, we obtain a local version of Isomap for which the minimization of the stress may also be used for parameter tuning.

## 1 Introduction

This paper considers the embedding problem in its two main forms: multidimensional scaling and manifold learning. Multidimensional scaling (MDS), is also known as, or at least closely related to, graph drawing, graph realization, and sensor network localization, and consists in positioning items as points in a Euclidean space of given dimension, preserving as much as possible the available proximity information. Manifold learning, often synonymous with nonlinear dimensionality reduction (DR), aims at embedding the available data points into a lower-dimensional space while preserving, as much as possible, the pairwise intrinsic distances. As is well-known, the two problems are closely related, even as they are not the same. We will mostly consider the MDS problem, and later derive implications for DR.

Many methods for embedding data necessitate the specification of one or several parameters, and being the situation unsupervised in that the items (in MDS) or the points (in DR) are not labeled, it is not obvious how to tune these parameters. In fact, we are not aware of any data-driven procedures for choosing such parameters that are currently in use. There is no equivalent to

---

This work was partially supported by the US National Science Foundation (DMS 1916071).

\*Department of Mathematics, University of California, San Diego, USA  
<https://math.ucsd.edu/~eariasca>

†Department of Mathematics, University of California, San Diego, USA  
<https://math.ucsd.edu/people/graduate-students/>

cross-validation — a widely used method for parameter tuning in the context of supervised learning such as regression or classification — that we know of.

We propose a simple approach: to use a notion of stress — a measure of quality of fit — to supervise the choice of tuning parameters. The use of the stress is rather natural, but the rationale for its use is quite distinct from the one supporting the use of, say, cross-validation in regression.

## 1.1 Tuning parameters

Using distances, or more generally, dissimilarities, to acquire a configuration of points in Euclidean space is a well-known problem that bears the name *multidimensional scaling (MDS)* in statistics [12]. We are given some pairwise dissimilarities on  $n$  items that we want to embed as points in a given Euclidean space while preserving dissimilarities as much as possible.

The field was first developed by psychologists seeking to analyze some of their data, and among these was Warren Torgerson, who in his thesis proposed a method now known as *classical scaling (CS)* or *Torgerson scaling* [64], which remains the most popular method for MDS to this day.

Just like *principal component analysis (PCA)* — its counterpart in the area of dimensionality reduction proposed fifty years earlier by Karl Pearson [43] — CS is parameter-free: it does not require the selection of any tuning parameter assuming the embedding dimension is provided by the user. Other popular methods such as the more recent *SMACOF* [21] are also parameter-free.

However, other prominent methods for MDS do require the choice of tuning parameters. An example of such a method is *MDS-MAP(P)* [53], a method that stitches together overlapping patches embedded by CS. Like any other method in its class, the patch size needs to be chosen carefully as it controls how local the method is. We use MDS-MAP(P) as a prototypical algorithm to showcase how a tuning parameter can be selected in MDS.

*Remark 1.1.* Although the embedding dimension may be seen as a tuning parameter, we will consider the embedding dimension to be given throughout the paper until the very end in Section 6.1. We do so because the choice of dimension is distinct from the choice of other tuning parameters.

## 1.2 Minimizing the stress

While Torgerson’s method is known to minimize an objective function known as the *strain*, more recent work has focused on MDS methods that minimize what is known as the *stress* — a cost function that measures the discrepancy between the provided dissimilarities and the Euclidean distances of the embedded points. It plays the role that the mean squared error plays in regression. Direct minimization of the stress — sometimes called *least squares scaling* — is the equivalent of least squares regression, but unlike the latter, the former presents formidable computational challenges: the aforementioned SMACOF employs a majorization approach, while MDS-MAP(P) uses a divide-and-conquer strategy consisting in embedding small subsets of items and then aligning the resulting partial embeddings.

In regression, it is well-known that optimizing the MSE is not a useful way to select a tuning parameter as it mostly leads to overfitting. For example, in kernel regression, optimizing the MSE leads to selecting a value of the bandwidth that is so small that the data is interpolated.<sup>1</sup> The situation in MDS is different in that minimizing the stress does not lead to overfitting. This

---

<sup>1</sup>This assumes that all the values of the predictor variable in the data are distinct and that the kernel being used is compactly-supported, although the claim remains essentially true when using other kernel functions such as the Gaussian kernel.

may be explained by the fact any method for MDS is constrained to return a configuration of points in a Euclidean space, where the pairwise distances have a very particular structure, and this constraint effectively limits the (statistical) complexity of the method. (Overfitting may arise when selecting the embedding dimension. We will discuss that separately at the very end of the article in Section 6.1.)

### 1.3 Bias–variance tradeoff

In our investigation into the selection of tuning parameters for patch–stitching methods for MDS, we also uncover what could be appropriately called a *bias–variance tradeoff*. While such a tradeoff is well-known in regression [30, Ch 7] — where it is foundational in the textbook understanding of statistical complexity and the need to appropriately select method parameters — the discussion of such a phenomenon appears to be absent from the MDS literature.

Our numerical experiments show that minimizing the stress helps strike a seemingly good compromise between bias and variance in situations such as in sensor network localization, where the sensors span a non-convex region of space and the dissimilarities are noisy versions of the Euclidean distances between the sensors.

### 1.4 Content

The remainder of the paper is organized as follows. In Section 2, we more formally describe the MDS embedding problem, we review some methods including MDS-MAP(P), and we introduce the stress and discuss its use for parameter selection. Some elements of theory are provided in Section 3. Some numerical experiments are presented in Section 4. This is where we discuss the bias–variance phenomenon mentioned above. In Section 5, we turn to dimensionality reduction, where we adapt MDS-MAPS(P) into a method for manifold learning akin to a local form of *Isomap* [59, 62], and show that the stress can also be used for parameter tuning. Section 6 is a discussion section.

## 2 Parameter selection in multidimensional scaling

### 2.1 Positioning problem

In multidimensional scaling (MDS), we are provided with some pairwise dissimilarities between a number of items, and the general goal is to embed these items as points in a Euclidean space of given dimension while preserving, as much as possible, the dissimilarity information.

More formally, we are given an undirected graph  $\mathcal{G} = (\mathcal{V}, \mathcal{E})$ , with node set  $\mathcal{V} = [n] := \{1, \dots, n\}$  and edge set  $\mathcal{E} \subset \mathcal{V} \times \mathcal{V}$ , together with non-negative weights on the edges. The weight on  $(i, j) \in \mathcal{E}$  is referred to as the dissimilarity between  $i$  and  $j$ , and denoted  $d_{ij}$ . The (possibly incomplete) matrix  $D = (d_{ij})$  stores the available information. Based on this information, we seek to embed the nodes or items into a Euclidean space of given dimension, say,  $\mathbb{R}^p$ , meaning that we seek  $y_1, \dots, y_n \in \mathbb{R}^p$  such that  $\|y_i - y_j\| \approx d_{ij}$ . The stress, defined below, offers a way to quantify the accuracy of the approximation. We say that the graph is *realizable* (in dimension  $p$ ) if there is a point set  $y_1, \dots, y_n \in \mathbb{R}^p$  such that  $\|y_i - y_j\| = d_{ij}$  for all  $(i, j) \in \mathcal{E}$ .

*Remark 2.1.* The positioning is necessarily up to a rigid transformation, as such a transformation does not change the pairwise Euclidean distances. However, positions in a global reference frame may be obtained if anchors, or points with known coordinates, are provided. We will not deal with this situation here.

Traditionally,  $p = 2$ , to facilitate a direct visualization of the data, but other values are certainly possible. In some applications,  $p = 2$  is the natural choice, an important example of which is wireless sensor networks where GPS is unavailable but communication between nearby sensors is possible via radio [7, 8, 15, 49, 55]. In any case, as announced in Remark 1.1, we assume that the embedding dimension is given, and only discuss its selection at the end of the paper in Section 6.1, as it is distinct from the selection of the kind of tuning parameters that we consider in the main body of the paper.

**Sensor network localization** In our theoretical study in Section 3 and in our numerical experiments presented in Section 4, we will focus on the *sensor network localization* setting, which we define to be a realizable setting with noise. When developing theory in Section 3, we follow Anderson et al. [1] and Javanmard and Montanari [32], and consider an additive noise model of the form

$$d_{ij}^2 = \|x_i - x_j\|^2 + \varepsilon_{ij}, \quad (2.1)$$

where  $x_1, \dots, x_n \in \mathbb{R}^p$  and  $\{\varepsilon_{ij} : (i, j) \in \mathcal{E}\}$  represent stochastic measurement noise. In our numerical experiments, we use a multiplicative noise model, which is a special of (2.1). This is a compelling mathematical setting as it models important applications and also allows one to visualize how well methods perform by comparing the embedded points  $y_1, \dots, y_n$  with the underlying points  $x_1, \dots, x_n$ , after an alignment.

## 2.2 Positioning methods

We review a few key approaches to MDS that will play a special role in the article. This review is purposefully not comprehensive, and in particular we leave out a number of important methods, including the whole class of semidefinite programming methods [11, 32, 61, 69].

**Classical scaling** This method — proposed by Torgerson [64, 65] and further developed by Gower [29] — takes a spectral approach that relies on a theorem by Schoenberg [50]. The method is detailed in Algorithm 1. The method is known to be exact in a realizable setting, and in general, it is known to minimize the (raw) strain, defined as

$$\sum_{i < j} (\langle y_i, y_j \rangle - b_{ij})^2, \quad (2.2)$$

where the  $b_{ij}$  are defined in Step 2 of the algorithm. Although minimizing the strain is not particularly intuitive, CS is known to behave well, at least in situations that are not too far from being realizable [4].

**Least squares scaling: SMACOF** Instead of the strain, it seems more appropriate to aim at minimizing the (raw) stress, here defined as

$$\sum_{(i,j) \in \mathcal{E}} (\|y_i - y_j\|^2 - d_{ij}^2)^2. \quad (2.3)$$

For a comparison of the strain and the stress, see [25]. Note that many other notions could play the same role of quantifying the accuracy of an embedding, but this particular choice is popular among authors contributing theory to the problem. Another popular variant is the same one but without

---

**Algorithm 1: Classical Scaling**


---

**Data:** Distance matrix  $D \in \mathbb{R}^{n \times n}$ , embedding dimension  $p$

**Result:** Configuration  $y_1, \dots, y_n \in \mathbb{R}^p$

- 1 Form the matrix  $A = (a_{ij})$  with  $a_{ij} := -\frac{1}{2}d_{ij}^2$ ;
  - 2 Double-center  $A$  to obtain  $B = (b_{ij})$  with  $b_{ij} := a_{ij} - \bar{a}_{i.} - \bar{a}_{.j} + \bar{a}_{..}$ ;
  - 3 Compute the top  $p$  eigenvectors of  $B$ , denoted  $u_1, \dots, u_p$  and ordered according to the eigenvalues  $\nu_1 \geq \dots \geq \nu_p$ ;
  - 4 Return  $y_i := (\sqrt{\nu_1^+}u_{i,1}, \dots, \sqrt{\nu_p^+}u_{i,p}) \in \mathbb{R}^p$ , where  $\nu^+ = \max(\nu, 0)$  and  $u_j = (u_{1,j}, \dots, u_{n,j})$ ;
- 

squares inside, meaning,  $\sum_{(i,j) \in \mathcal{E}} (\|y_i - y_j\| - d_{ij})^2$ . It takes an entire class of methods to attempt to minimize the stress as it is non-convex and invariably high-dimensional — the minimization happens in dimension  $n \times p = np$  to be precise. The class of methods includes Kruskal’s steepest descent [36] algorithm and the Levenberg–Marquardt algorithm [67]. But among least squares scaling methods, the majorization method known as SMACOF proposed by de Leeuw and Mair [21] is particularly popular. As implemented in the eponymous R package, CS is used as an initialization when possible (meaning, when all dissimilarities are available).

**Completion by shortest path: MDS-D** In principle, SMACOF can tackle the minimization of the stress (2.3) even when some dissimilarities are not available. But in that case CS cannot be used for initialization, and it is not clear what to replace it with. This is not specified in [21], and we take this to mean that SMACOF is really best as a refinement procedure.

One of the first methods suggested for the in the incomplete setting is the *MDS-D* method of Kruskal and Seery [37]. It consists in replacing the missing dissimilarities with the graph distances and then applying CS to the completed dissimilarity matrix. Although simple, the method is known to perform well in the realizable setting where the underlying points are densely packed inside a convex set in the embedding space [2, 5, 10, 42]. It was rediscovered a number of times, including in the form of the *MDS-MAP* method of Shang et al. [54].

**Patch–stitching methods: MDS-MAP(P)** In the realizable setting where the underlying points cover a non-convex set, MDS-D or MDS-MAP do not work well as they produce a distorted embedding. To remedy the situation, Shang and Ruml [53] proposed to localize the method by first embedding neighborhood subgraphs by MDS-MAP obtaining partial embeddings called *patches*, and then stitching these together to form a global embedding or map. The method defines the neighborhood by number of ‘hops’, and this is the only parameter of the method when the embedding dimension is given (see Remark 1.1). See Figure 2.1 for a visualization of the patches and their sequential stitching. We use this method to illustrate, in our experiments, the use of the stress for parameter selection, and for this reason, we detail the method in Algorithm 2 in a somewhat simplified form. (The variant proposed in [53] weighs connections according to the number of hops and uses these weights in the refinement step. See, also, [18].)

In terms of computational complexity, the Floyd–Warshall algorithm [28] runs in  $O(k^3)$  time on a graph with  $k$  nodes and is used in Step 4 to calculate all pairs of shortest path distances for each neighborhood. This is the main computational bottleneck. Some improvement may be possible using an algorithm that is able to exploit the sparsity of  $D_v$  [45, 48]. Classical scaling is used in Step 5. Using a naive eigendecomposition results in a complexity of  $O(k^3)$  for  $k \times k$  matrices, but there are approximate algorithms that run in linear time [22, 70]. The stitching in Step 12 is done by Procrustes, while the refinement in Steps 6 and 14 is done by SMACOF. (The final SMACOF

**Algorithm 2:** MDS-MAP(P)

---

**Data:** Weighted graph  $\mathcal{G} = (\mathcal{V}, \mathcal{E}, D)$ , number of hops  $h$ , embedding dimension  $p$   
**Result:** Configuration  $y_1, \dots, y_n \in \mathbb{R}^p$

- 1 **for**  $v \in \mathcal{V}$  **do**
- 2      $N_v \leftarrow h$ -hop neighborhood of  $v$ ;
- 3      $D_v \leftarrow D[N_v, N_v] = (d_{ij} : i, j \in N_v; (i, j) \in \mathcal{E})$ ;
- 4      $\Lambda_v \leftarrow$  MDS-D applied to  $D_v$ ;
- 5      $X_v \leftarrow$  CS applied to  $\Lambda_v$ ;
- 6      $X_v \leftarrow$  refinement of  $X_v$ ;
- 7 **end**
- 8  $Y \leftarrow \arg \max_{X_v} \text{card}(N_v)$ ;
- 9  $N_Y \leftarrow N_v$ ;
- 10 **while** *there exist unmapped nodes* **do**
- 11      $X_{v^*} \leftarrow \arg \max_{X_v} \text{card}(N_v \cap N_Y)$ ;
- 12      $Y \leftarrow \text{merge}(Y, X_{v^*})$ ;
- 13 **end**
- 14  $Y \leftarrow$  refinement of  $Y$ ;
- 15 Define and return  $y_1, \dots, y_n$ , the row vectors of  $Y$ ;

---

refinement is an optional step that can be extremely costly for large datasets. It can be useful when the number of patches is relatively small.)



Figure 2.1: In the MDS-MAP(P) algorithm, each patch is embedded separately and then merged sequentially. The points in the seed patch are in dark blue, while points added with subsequent patches are more and more red as the stitching progresses. Plotted above are embeddings with number of hops  $h = 1, 2, 5$ .

There is an entire class of patch–stitching methods [19, 24, 35, 38, 60, 71]. We only choose to work with MDS-MAP(P) because we find it simple.

### 2.3 Parameter tuning by stress minimization

The approach we propose for choosing one or even several tuning parameters, such as the number of hops in MDS-MAP(P), consists in minimizing the stress (2.3). The stress has the role of empirical risk, and it may thus be surprising, when comparing to the situation in regression, that it can be used for parameter selection. But this is indeed the case, and can be explained by the fact that, as long as the embedding dimension  $p$  is given, the requirement that a method needs to return an embedding in  $\mathbb{R}^p$  is enough to cap the statistical complexity so that overfitting is not possible: in

fact, we want to come as close as possible to realizing the graph. (The situation is very different when choosing the embedding dimension; see Section 6.1.)

### 3 Theory

In the sensor network localization framework (2.1), the stress clearly functions as a proxy for the *noiseless stress*, defined as

$$\sum_{(i,j) \in \mathcal{E}} (\|y_i - y_j\|^2 - \|x_i - x_j\|^2)^2. \quad (3.1)$$

In turn, the noiseless stress functions as a proxy for the *complete noiseless stress*, defined as

$$\sum_{i < j} (\|y_i - y_j\|^2 - \|x_i - x_j\|^2)^2. \quad (3.2)$$

We examine below how the stress tracks the complete noiseless stress. We will see that, while the relationship is not perfect, they do tend to track each other. But at a conceptual level, how can this be anticipated?

#### 3.1 Rigidity theory

To investigate this, we turn to *rigidity theory*, which examines the question of uniqueness (up to a rigid transformation) when realizing a weighted graph in a given Euclidean space [6, 39, 63]. We introduce some vocabulary from that literature (in particular, from [17]). A *configuration* is a set of  $n$  points in  $\mathbb{R}^p$  indexed by  $[n] = \{1, \dots, n\}$ . A configuration is *generic* if the set of its coordinates do not satisfy any nonzero polynomial equation with integer coefficients. We say that two configurations  $\mathbf{y} = \{y_1, \dots, y_n\}$  and  $\mathbf{z} = \{z_1, \dots, z_n\}$  are *congruent* if there is a rigid transformation  $f: \mathbb{R}^p \rightarrow \mathbb{R}^p$  such that  $z_i = f(y_i)$  for all  $i \in [n]$ . A configuration  $\mathbf{y} = \{y_1, \dots, y_n\}$  and a graph  $\mathcal{G} = (\mathcal{V} = [n], \mathcal{E})$ , together, form a *framework*, denoted  $\mathcal{G}(\mathbf{y})$ . We say that two frameworks,  $\mathcal{G}(\mathbf{y})$  and  $\mathcal{G}(\mathbf{z})$  are *equivalent* if

$$\|y_i - y_j\| = \|z_i - z_j\|, \quad \forall (i, j) \in \mathcal{E}. \quad (3.3)$$

The framework  $\mathcal{G}(\mathbf{y})$  is said to be *globally rigid* if, whenever  $\mathcal{G}(\mathbf{y})$  and  $\mathcal{G}(\mathbf{z})$  are equivalent, then necessarily  $\mathbf{y}$  and  $\mathbf{z}$  are congruent. The graph  $\mathcal{G}$  is said to be *generically globally rigid* if  $\mathcal{G}(\mathbf{y})$  is globally rigid whenever  $\mathbf{y}$  is generic.

The complete noiseless stress (3.2) is exactly zero when  $\|y_i - y_j\| = \|x_i - x_j\|$  for all  $i < j$ , and we know this to be equivalent to  $\mathbf{y} = \{y_1, \dots, y_n\}$  and  $\mathbf{x} = \{x_1, \dots, x_n\}$  being congruent. For the noiseless stress (3.1), the same is true if  $\mathcal{G}(\mathbf{x})$  is globally rigid. This is by mere definition, and we would like to know when this happens. Also by definition, it happens when  $\mathbf{x}$  is a generic configuration and  $\mathcal{G}$  is *generically globally rigid*.

Generic configurations are ‘common’ in that those that are not have zero Lebesgue measure (in  $\mathbb{R}^{np}$ ). This is simply because there are countably many polynomials with integer coefficients and each one of these defines a surface via its null set of zero Lebesgue measure. In particular, if a configuration is drawn iid at random from a distribution with a density then the configuration is generic with probability one.

The latter question, about whether a graph is generically globally rigid or not, is a more delicate question. In the very special, but useful case of  $p = 2$ , Jackson and Jordán [31] have shown that if the graph is 6-vertex connected, meaning that it remains connected even after the removal of any 5 vertices, then the graph is generically globally rigid. The situation in dimension  $p \geq 3$  is more complex.

### 3.2 Sequential trilateration

Aspnes et al. [7] (starting with an earlier version [26]) propose a useful simplification. They consider the notion of *trilateration graph* (in dimension  $p$ ), which they define as a graph with  $n \geq p+1$  vertices that admits an ordering of its vertices, say  $v_1, \dots, v_n$ , such that the subgraph induced by  $v_1, \dots, v_{p+1}$  is complete and, for each  $j > p+1$ ,  $v_j$  is connected to at least  $p+1$  vertices among  $v_1, \dots, v_{j-1}$ . Aspnes et al. call this a *trilaterative ordering* (in dimension  $p$ ). The name comes from the fact that such a graph, combined with a configuration in general position (meaning that any  $(p+1)$ -tuple from the configuration has affine span the entire space), forms a framework which is realizable by sequential trilateration.

Fang et al. [27] generalize this notion to graphs whose configurations are *sequentially localizable*. Working in dimension two, they show that the two notions are distinct, but closely related nonetheless.

**Random geometric graphs** In sensor network localization, it is common to model the network as a *random geometric graph* [44]. Such a graph has node set representing points that are drawn iid from some distribution on  $\mathbb{R}^p$  and edges between any two of these points within distance  $r$ . For example, Aspnes et al. [7] show that, for the uniform distribution on  $[0, 1]^2$ , as the size of the configuration increases, if the connectivity radius is not too small, the probability that the resulting graph is generically globally rigid, and that the corresponding framework is rigid, tends to one. We generalize their result.

**Theorem 3.1.** *Suppose a configuration of cardinality  $n$  is drawn iid from a density supported on  $\bar{\Omega} \subset \mathbb{R}^p$ , where  $\Omega$  is bounded, open, and connected. Considering the asymptotic regime  $n \rightarrow \infty$ , there is  $r_n \rightarrow 0$  such that a graph built on this configuration with a connectivity radius  $r \geq r_n$  is a trilateration graph with probability tending to one.*

The conditions on the support of the distribution generating the locations of the sensors are very mild. ( $\bar{\Omega}$  is the closure of  $\Omega$ , and is necessary since the support of a distribution is a closed set by definition.) Given that the points are sampled from a density, if the graph is a trilateration graph then it is also true with probability one that the corresponding framework is rigid.

*Proof.* Let  $\mathcal{G}_r(\mathbf{x})$  be the neighborhood graph with connectivity radius  $r$  built on the point set  $\mathbf{x} = \{x_1, \dots, x_n\}$ . It is obvious that the property of being a trilateration graph is monotonic in  $r$  in the sense that if  $\mathcal{G}_r(\mathbf{x})$  is a trilateration graph then so is  $\mathcal{G}_s(\mathbf{x})$  for any  $s > r$ . It therefore suffices to find  $r_n \rightarrow 0$  such that  $\mathcal{G}_{r_n}(x_1, \dots, x_n)$  is trilateration graph with probability tending to 1. (All limits are as  $n \rightarrow \infty$  unless otherwise specified.)

$\Omega$  being bounded, for any  $m \geq 1$  integer, it can be covered with finitely many, say  $N_m$ , open balls of radius  $1/2m$  and with center a point in  $\Omega$ . (We even know that the minimum number  $N_m$  satisfies  $N_m \leq C_0 m^p$ , where  $C_0$  depends on  $\text{diam}(\Omega)$  and  $p$ , although this will not play a role in what follows.) We consider such a covering, with balls denoted  $B_1^m, \dots, B_{N_m}^m$ , and assume that all the balls in the covering intersect  $\Omega$ , meaning that  $A_j := B_j \cap \Omega \neq \emptyset$  for all  $j$ . Form the following graph: the node set is  $A_1^m, \dots, A_{N_m}^m$ , and  $A_j^m$  and  $A_k^m$  are connected if they intersect. We call this the *cover graph*. Because  $\Omega$  is connected, the cover graph must also be connected, and may therefore be traversed by, say, depth-first search, which starting at any  $A_{j_0}^m$  results in a (finite) path in the cover graph that passes through the entire graph, meaning, a sequence  $(A_{j_s}^m : s = 0, \dots, S_m)$  with  $I_s^m := A_{j_{s-1}}^m \cap A_{j_s}^m \neq \emptyset$  for all  $s$ , with the property that, for any  $j$ , there is  $s$  such that  $A_{j_s}^m = A_j^m$ . Note that, by construction, each  $I_s^m$  is a nonempty open subset of  $\Omega$  of diameter  $< 1/m$ ; together, these subsets cover  $\Omega$ . (Note that some of these sets might coincide, but this is unimportant.)

Now, let  $f$  be a density with support  $\bar{\Omega}$ , and let  $x_1, \dots, x_n$  denote an iid sample from  $f$ . For a Borel set  $A$ , let  $P(A) = \int_A f$ . Consider the event  $E_s^{n,m}$  that  $I_s^m$  contains at least  $p+1$  sample points, and define  $E^{n,m} = \cap_s E_s^{n,m}$ , which is the event that each one of the subsets  $I_1^m, \dots, I_{S_m}^m$  contains at least  $p+1$  sample points. Let  $a(n, m) = 1 - \mathbb{P}(E^{n,m})$ , which is the probability that  $E^{n,m}$  fails to happen. Note that, essentially by definition,  $a(n, m)$  is decreasing in  $n$ . In addition to that, we also have  $\lim_{n \rightarrow \infty} a(n, m) = 0$ . To see this, we derive, by the union bound and the fact that the number of points falling in a Borel set  $A$  is binomial with parameters  $n$  and  $P(A)$ ,

$$a(n, m) \leq \sum_{s=0}^{S_m} \mathbb{P}(\text{not } E_s^{n,m}) \quad (3.4)$$

$$\leq \sum_{s=0}^{S_m} \sum_{k=0}^p \binom{n}{k} P(I_s^m)^k (1 - P(I_s^m))^{n-k} \quad (3.5)$$

$$\leq (S_m + 1)(p + 1)n^p (1 - b_m)^{n-p}, \quad b_m := \min_{s=0, \dots, S_m} P(I_s^m). \quad (3.6)$$

Since each  $I_s^m$  is a nonempty open subset of  $\Omega$ , we have that  $b_m > 0$ , and so  $a(n, m) \rightarrow 0$  as  $n \rightarrow \infty$  when  $m$  remains fixed. (The convergence is even exponentially fast, although this will not play a role.) The fact that  $a(n, m)$  is decreasing in  $n$  and  $\lim_{n \rightarrow \infty} a(n, m) = 0$  implies, via elementary arguments, that there is sequence  $m_n \rightarrow \infty$  such that  $\lim_{n \rightarrow \infty} a(n, m_n) = 0$ , or equivalently,  $\mathbb{P}(E^{n, m_n}) \rightarrow 1$  as  $n \rightarrow \infty$ .

We now prove that, under  $E^{n, m}$ , the neighborhood graph built on the sample points  $x_1, \dots, x_n$  with connectivity radius  $r = 1/m$  is a trilateration graph. Thus, we work under the situation where each  $I_s^m$  contains at least  $p+1$  sample points. First, consider  $p+1$  such points in  $I_1^m$ , and label them  $v_1, \dots, v_{p+1}$  in any order. Since  $\text{diam}(I_1^m) < r$ , the subgraph that these points induce is complete. Recall that  $I_1^m \subset A_{j_0}^m$ . Label the remaining points in  $A_{j_0}^m$  as  $v_{p+1}, \dots, v_{n_0}$  and note that, since  $\text{diam}(A_{j_0}^m) < r$ , each of these points is connected to all the points  $v_1, \dots, v_{p+1}$ . Let  $\mathcal{V}_0$  denote  $\{v_1, \dots, v_{n_0}\}$ . Similarly, recall that  $I_1^m \subset A_{j_1}^m$ ; label the remaining points in  $A_{j_1}^m$  as  $v_{n_0+1}, \dots, v_{n_1}$ , and note that, since  $\text{diam}(A_{j_1}^m) < r$ , each of these points is connected to all the points  $v_1, \dots, v_{p+1}$ , and therefore to at least  $p+1$  points inside  $\mathcal{V}_0$ ; let  $\mathcal{V}_1 := \{v_1, \dots, v_{n_1}\}$ . Suppose that we are at a stage where we have built an ordering  $\mathcal{V}_{s-1} = \{v_1, \dots, v_{n_{s-1}}\}$  of the sample points in  $A_{j_0}^m, \dots, A_{j_{s-1}}^m$  such that, for each  $p+1 < j \leq j_{s-1}$ ,  $v_j$  is connected to at least  $p+1$  points among  $v_1, \dots, v_{j-1}$ . In particular, this includes all the points in  $I_s^m$  since  $I_s^m \subset A_{j_{s-1}}^m$ . Now,  $I_s^m \subset A_{j_s}^m$  also; label the remaining points in  $A_{j_s}^m$  as  $v_{n_{s-1}+1}, \dots, v_{n_s}$ , and since  $\text{diam}(A_{j_s}^m) < r$ , each of these points is connected to all the points  $I_s^m$ . Since  $I_s^m$  contains at least  $p+1$  points (because  $E^{n,m}$  holds), we may continue the recursion by letting  $\mathcal{V}_s = \{v_1, \dots, v_{n_s}\}$ . Doing so until all the sample points have been processed provides a trilaterative ordering of the entire neighborhood graph  $\mathcal{G}_r(x_1, \dots, x_n)$ .  $\square$

### 3.3 Rigidity theory in the presence of noise

What we have learned so far is that, if the graph  $\mathcal{G} = (\mathcal{V}, \mathcal{E})$  given in the embedding problem is generically globally rigid, and we are in a realizable situation with an underlying configuration  $x_1, \dots, x_n$  that is generic, then the noiseless stress (3.1) is minimized exactly where the complete noiseless stress (3.2) is minimized, that is, at all the rigid transformations of the configuration. We also know that these conditions are fulfilled (with high probability) for common sensor network models such as random geometric graphs (Theorem 3.1). But it does not imply much about the noisy stress (2.3), in general.

While most of the literature on rigidity theory focuses on the noiseless setting, Anderson et al. [1] consider the question of stability in the presence of noise. They do so in the realizable setting

in dimension  $p = 2$ , and in presence of *anchors*, which are points whose position is known. The graph is generically globally rigid with an underlying generic configuration. With anchors, the configuration is effectively unique, not just up to a rigid transformation. In this context, [Anderson et al.](#) show that the distance between the minimizer of the stress (2.3) constrained by the anchors and the underlying configuration is bounded by a constant multiple of the noise amplitude.

We prove an analogous result in the present (more complex) anchor-free setting for an arbitrary embedding dimension. We do so for trilateration graphs, which as we know from Theorem 3.1 covers important models, and also allow us to offer a completely different proof based on a new stability result for the sequential trilateration approach of Aspnes et al. [7], which we establish by leveraging stability results for CS and a form of trilateration available in our previous work [4].

**Theorem 3.2.** *Consider a sensor network localization situation (2.1) in which the network structure is a trilateration graph and the configuration is in general position. Then, there is  $\sigma > 0$  and  $C > 0$  such that, if  $\sum_{(i,j) \in \mathcal{E}} \varepsilon_{ij}^2 \leq \sigma^2$ , the following holds: any minimizer  $(y_1^*, \dots, y_n^*)$  of the stress (2.3) satisfies*

$$\min_T \sum_{i \in [n]} \|y_i^* - Tx_i\|^2 \leq C \sum_{(i,j) \in \mathcal{E}} \varepsilon_{ij}^2, \quad (3.7)$$

where the minimization is over the rigid group of transformations.

As in [1], the constants  $\sigma$  and  $C$  depend on the network structure and the configuration, namely, on the framework  $\mathcal{G}(\mathbf{x})$ . We do assume that  $\sigma \leq 1$ , which is without loss of generality. Just like [Anderson et al.](#), we make no effort to optimize these constants in our proof, which occupies the remaining of the section.

The following is a stability result for CS.

**Lemma 3.3** (Corollary 2 in [4]). *Consider a configuration  $x_1, \dots, x_m \in \mathbb{R}^p$  spanning the entire space, and a set of dissimilarities  $(d_{ij})$ , and define*

$$\eta^4 = \sum_{i < j} (d_{ij}^2 - \|x_i - x_j\|^2)^2. \quad (3.8)$$

Then there are constants  $\eta_0 > 0$  and  $C_0 > 0$  depending on the configuration such that, if  $\eta \leq \eta_0$ , then CS with input dissimilarities  $(d_{ij})$  (and given dimension  $p$ ) returns a configuration  $y_1, \dots, y_m$  satisfying

$$\min_T \sum_{i \in [m]} \|y_i - Tx_i\|^2 \leq C_0 \eta^4, \quad (3.9)$$

where the minimization is over the rigid group of transformations.

We note that Aspnes et al. [7] do not propose a particular method for trilateration. We use a variant proposed by de Silva and Tenenbaum [22], described in Algorithm 3, which is based on approaching the problem via inner products. It is exact in the realizable case. The following is a stability result for this trilateration method, where stability is considered with respect to noise both at the level of the dissimilarities and at the level of the landmarks.

**Lemma 3.4** (Corollary 3 in [4]). *Consider a configuration  $x_1, \dots, x_m \in \mathbb{R}^p$  spanning the entire space. Let  $y_1, \dots, y_m \in \mathbb{R}^p$  be another configuration and let  $d_1, \dots, d_m$  be set of dissimilarities. For a point  $x$ , define*

$$\nu^2 = \sum_{i \in [m]} \|y_i - x_i\|^2, \quad \eta^4 = \sum_{i \in [m]} (d_i^2 - \|x - x_i\|^2)^2. \quad (3.10)$$

**Algorithm 3:** Trilateration [22]**Data:** landmarks  $y_1, \dots, y_m$ , dissimilarities  $d_1, \dots, d_m$ **Result:** point  $y$ 

- 1 Square the dissimilarities to form  $d^{\circ 2} = (d_1^2, \dots, d_m^2)$ ;
- 2 Compute  $a = (a_1, \dots, a_m)^\top$  where  $a_j = \frac{1}{m} \sum_{i=1}^m \|y_i - y_j\|^2$ ;
- 3 Compute the pseudo-inverse  $Y^\ddagger$  where  $Y = [y_1 \dots y_m]^\top$ ;
- 4 Return  $y = \frac{1}{2} Y^\ddagger (a - d^{\circ 2})$ ;

Then there are constants  $\nu_0 > 0$  and  $C_0 > 0$  depending on the configuration  $x_1, \dots, x_m$  such that, if  $\nu \leq \nu_0$ , trilateration with inputs  $y_1, \dots, y_m$  and  $d_1, \dots, d_m$  returns  $y$  satisfying

$$\|y - x\|^2 \leq C_0(\nu^2 + \eta^4). \quad (3.11)$$

In the statement,  $x_1, \dots, x_m$  play the role of landmarks and  $x$  is the unknown point to be recovered;  $y_1, \dots, y_m$  should be seen as noisy versions of  $x_1, \dots, x_m$ , and  $d_1, \dots, d_m$  should be seen as noisy versions of  $\|x - x_1\|, \dots, \|x - x_m\|$ ;  $y$  is the point returned by the algorithm based on inputs  $y_1, \dots, y_m$  and  $d_1, \dots, d_m$ .

As announced, we use these stability results (Lemmas 3.3 and 3.4) to establish a stability result for sequential trilateration, which may be of independent interest as such results are scarce. (Moore et al. [41], inspired by the earlier work of Eren et al. [26], propose a method for sequential trilateration and carry out a very limited mathematical analysis, restricting themselves to analyzing the probability of a gross error or ‘flip’ in one trilateration step. We are not aware of any other results.)

**Theorem 3.5.** *In the context of Theorem 3.2, a sequential trilateration results in an embedding that satisfies a bound of the form (3.7).*

An upper case  $C$  symbol, often subscripted, represents a constant that depends on the configuration that may change along the way.

*Proof.* Assume without loss of generality that  $1, \dots, n$  is already a trilaterative ordering. We therefore process the dissimilarities in the same order.

Therefore, at initialization, we apply CS to  $(d_{ij} : 1 \leq i < j \leq p+1)$ , which we can do since these dissimilarities are available because of the assumption that  $1, \dots, n$  is a trilaterative ordering, and also the fact that no dissimilarity is missing. We let  $y_1, \dots, y_{p+1}$  be the output and use Lemma 3.3 to quantify its accuracy. In our situation,

$$\eta^4 = \sum_{1 \leq i < j \leq p+1} \varepsilon_{ij}^2 \leq C_1 \sigma^2. \quad (3.12)$$

Assuming  $\sigma$  is small enough that  $C_1 \sigma^2 \leq \eta_0^4$ , where  $\eta_0$  is (implicitly) given in Lemma 3.3, that same lemma gives that

$$\sum_{1 \leq i \leq p+1} \|y_i - T x_i\|^2 \leq C_2 \sum_{1 \leq i < j \leq p+1} \varepsilon_{ij}^2, \quad (3.13)$$

for some rigid transformation  $T$ . Henceforth, we assume that  $T$  is the identity transformation, which we can do without loss of generality. (We reinitialize the constants.)

Define  $\mathcal{E}_k = \{(i, j) \in \mathcal{E} : i, j \in [k]\} = \mathcal{E} \cap [k]^2$ , and assume that we have embedded  $y_{p+2}, \dots, y_{k-1}$  in such a way that, for some constant  $C$ ,

$$\sum_{1 \leq i \leq k-1} \|y_i - x_i\|^2 \leq C \sum_{(i,j) \in \mathcal{E}_{k-1}} \varepsilon_{ij}^2. \quad (3.14)$$

We are now poised to embed  $y_k$  by trilateration based on  $p+1$  points in  $\{y_1, \dots, y_{k-1}\}$  and the corresponding dissimilarities. Assume these points to be  $y_{i_1}, \dots, y_{i_{p+1}}$ , so that the corresponding dissimilarities are  $d_{k,i_1}, \dots, d_{k,i_{p+1}}$ , and  $y_k$  is the output of Algorithm 3 based on these inputs. We use Lemma 3.4 to quantify the accuracy of this embedding. In our situation, we have

$$\nu^2 = \sum_{j=1}^{p+1} \|y_{i_j} - x_{i_j}\|^2 \leq \sum_{1 \leq i \leq k-1} \|y_i - x_i\|^2 \leq C \sum_{(i,j) \in \mathcal{E}_{k-1}} \varepsilon_{ij}^2 \leq C_1 \sigma^2, \quad (3.15)$$

using our induction hypothesis (3.14) above. We assume that  $\sigma$  is small enough that  $C_1 \sigma^2 \leq \nu_0^2$ . And we also have

$$\eta^4 = \sum_{j=1}^{p+1} (d_{k,i_j}^2 - \|x_k - x_{i_j}\|^2)^2 = \sum_{j=1}^{p+1} \varepsilon_{k,i_j}^2 \leq \sum_{i=1}^{k-1} \varepsilon_{ki}^2. \quad (3.16)$$

The lemma then gives us the error bound

$$\|y_k - x_k\|^2 \leq C_0 \nu^2 + C_0 \eta^4 \leq C_0 C \sum_{(i,j) \in \mathcal{E}_{k-1}} \varepsilon_{ij}^2 + C_0 \sum_{i=1}^{k-1} \varepsilon_{ki}^2 \leq C_3 \sum_{(i,j) \in \mathcal{E}_k} \varepsilon_{ij}^2, \quad (3.17)$$

thus enabling us to continue the induction. At the end of the induction, when all the  $y_i$  have been embedded, we obtain the announced bound.  $\square$

So far, with Theorem 3.5, all we know is that sequential trilateration achieves a bound like (3.7), meaning that an output of sequential trilateration must satisfy

$$\sum_{i \in [n]} \|y_i - T x_i\|^2 \leq C \sum_{(i,j) \in \mathcal{E}} \varepsilon_{ij}^2, \quad (3.18)$$

for some rigid transformation  $T$ . We now leverage this to show that the same must be true of a minimizer of the stress, thus establishing Theorem 3.2.

We first bound the minimum value of the stress. Let  $y_1^*, \dots, y_n^*$  be a minimizer. Since  $x_1, \dots, x_n$  is feasible, it must be the case that the stress achieved by  $y_1^*, \dots, y_n^*$  is not larger than than the stress achieved by  $x_1, \dots, x_n$ , so that

$$\sum_{(i,j) \in \mathcal{E}} (\|y_i^* - y_j^*\|^2 - d_{ij}^2)^2 \leq \sum_{(i,j) \in \mathcal{E}} (\|x_i - x_j\|^2 - d_{ij}^2)^2 = \sum_{(i,j) \in \mathcal{E}} \varepsilon_{ij}^2. \quad (3.19)$$

Therefore, if we define  $\xi_{ij} = d_{ij}^2 - \|y_i^* - y_j^*\|^2$ , we have that

$$\sum_{(i,j) \in \mathcal{E}} \xi_{ij}^2 \leq \sum_{(i,j) \in \mathcal{E}} \varepsilon_{ij}^2. \quad (3.20)$$

Applying Theorem 3.5 with the same dissimilarities  $(d_{ij})$  and same graph structure but the configuration  $y_1^*, \dots, y_n^*$  instead of the configuration  $x_1, \dots, x_n$ , to obtain that an output of sequential trilateration  $y_1, \dots, y_n$  must satisfy

$$\sum_{i \in [n]} \|y_i - S y_i^*\|^2 \leq C \sum_{(i,j) \in \mathcal{E}} \xi_{ij}^2, \quad (3.21)$$

for some rigid transformation  $S$ . And this holds under an appropriately small upper bound on  $\sum_{(i,j) \in \mathcal{E}} \varepsilon_{ij}^2$ , as assumed in Theorem 3.2, because of (3.20). Using this and (3.18) with the upper bound (3.20), together with the triangle inequality, we thus have

$$\sum_{i \in [n]} \|y_i^* - Tx_i\|^2 \leq C_1 \sum_{(i,j) \in \mathcal{E}} \varepsilon_{ij}^2, \quad (3.22)$$

for some rigid transformation  $T$  — which concludes the proof of Theorem 3.2.

## 4 Experiments

### 4.1 Synthetic datasets

We start with some varied synthetic datasets that exemplify the sensor network localization setting of Section 2.1. We first describe how the datasets used in the experiments are constructed. The ground truth configuration is denoted by  $x_1, \dots, x_n \in \mathbb{R}^2$ . In all cases, these are chosen dense in a domain with varying shape. This is done by considering a fine square grid of points inside the domain to which we add some jitter. The added jitter is small and plays two roles: it makes the setting somewhat more generic and it also prevents some possible systematic bias to arise when computing shortest path distances in the graph. The jittered grid inside the domain gives the configuration. The graph structure is given by connecting each point to its  $k = 15$  nearest neighbors. The pairwise Euclidean distances between configuration points that are connected in the graph are then corrupted by multiplicative noise as follows

$$d_{ij} = (1 + \varepsilon_{ij}) \|x_i - x_j\|. \quad (4.1)$$

Note that this is a special case of the additive noise model of (2.1). We choose the  $\varepsilon_{ij}$  iid from the uniform distribution on  $[-\sigma, \sigma]$ , where the noise amplitude  $\sigma$  varies from experiment to experiment.

We work with some emblematic shapes: a rectangle in Figure 4.1; a hollow rectangle in Figure 4.2; a C-shaped domain in Figure 4.3; and an H-shaped domain or ‘dumbbell’ in Figure 4.4 and also in Figure 4.5 for different noise levels. For each dataset, we apply MDS-MAP(P) with different choices for the number of hops and track the (average) stress and the (average) embedding error. We align the output configuration with the true configuration by (orthogonal) Procrustes [51]. We work with rather sparse graphs to better showcase the result of applying MDS-MAP(P) with different choices for the number of hops.

**Bias–variance tradeoff** In the standard textbook exposition of statistical complexity such as [30, Ch 7], one is taught that, in the context of regression (including classification), as the model being fitted to the data increases in complexity, the bias decreases while the variance increases. Model complexity is often driven by one or several tuning parameters (e.g., the bandwidth in kernel regression), and a ‘good’ selection of these parameters is one that results in a ‘good’ compromise between bias and variance, often understood as being equivalent to minimizing the prediction error. In [30, Fig 7.1], we see that, as the model complexity increases, the empirical error (as measured on training data) decreases, while the prediction error (as measured on the test data) decreases at first but then increases — and a ‘good’ selection of model complexity would be so that the prediction error is at its minimum.

The discussion of such a bias–variance tradeoff, or the choice of model complexity, seems absent from the MDS literature, except for the choice of embedding dimension (see Section 6.1). But it is clearly observed in our experiments involving a non-convex domain, as in Figure 4.2 (hollow

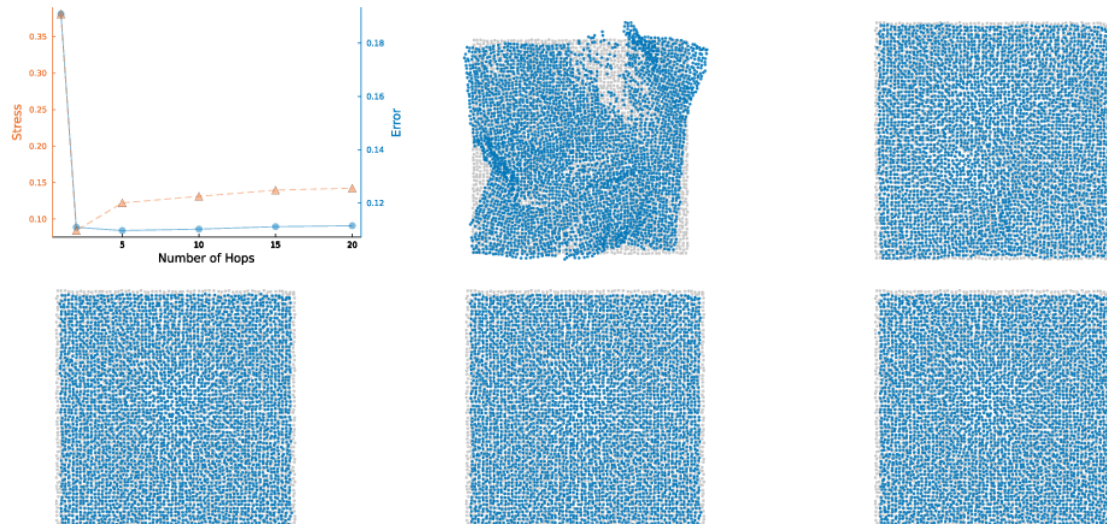


Figure 4.1: Experiment with  $n = 4000$  points on a rectangle with  $\sigma = 0.15$ . Top left: Comparison between stress and embedding error. In reading order, the remaining plots show the output of MDS-MAP(P) with number of hops  $h = 1, 2, 3, 5, 10$ .

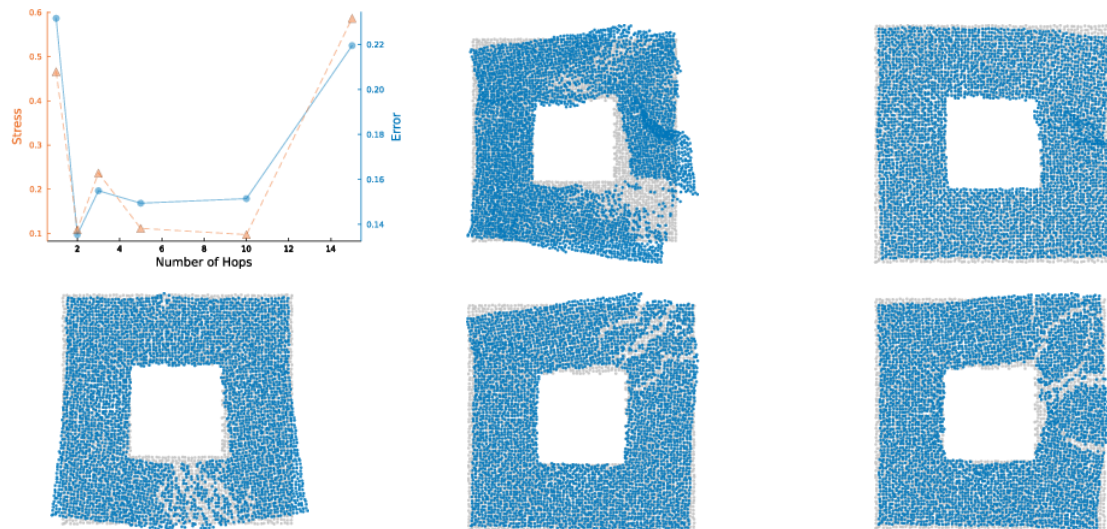


Figure 4.2: Experiment with  $n = 4140$  points on a rectangle with a rectangular hole with  $\sigma = 0.15$ . Top left: Comparison between stress and embedding error. In reading order, the remaining plots show the output of MDS-MAP(P) with number of hops  $h = 1, 2, 3, 5, 10$ .

rectangle), Figure 4.3 (‘C’ shape), and Figure 4.4 (‘H’ shape). Indeed, we can clearly see that, as the number of hops increases, the embedding error decreases and then increases. (As already argued in Section 2.3, the stress does not function as the empirical error does in regression because of the built-in Euclidean constraint. Otherwise, it would not be a good quantity to use for tuning.)

In the particular case of MDS-MAP(P), we may explain this as follows. When a domain is non-convex, using a large enough patch that covers the entire domain, MDS-MAP(P) coincides with MDS-D, and MDS-D is known to be biased unless the domain is convex. This is because the shortest path distances are consistent for the intrinsic distances [5, 10], and the intrinsic distances are not

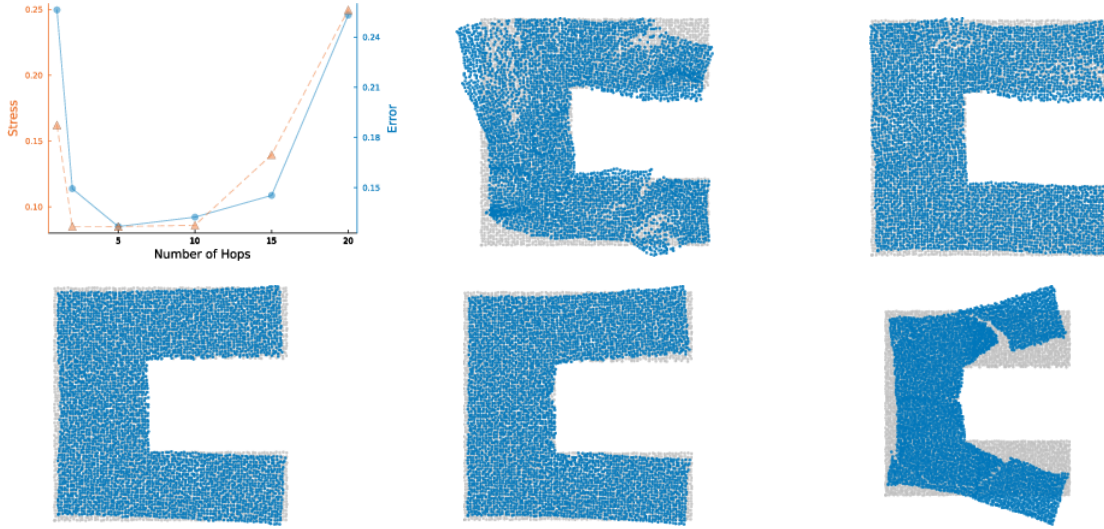


Figure 4.3: Experiment with  $n = 4528$  points on a C-shaped domain with  $\sigma = 0.15$ . Top left: Comparison between stress and embedding error. In reading order, the remaining plots show the output of MDS-MAP(P) with number of hops  $h = 1, 2, 5, 10, 20$ .

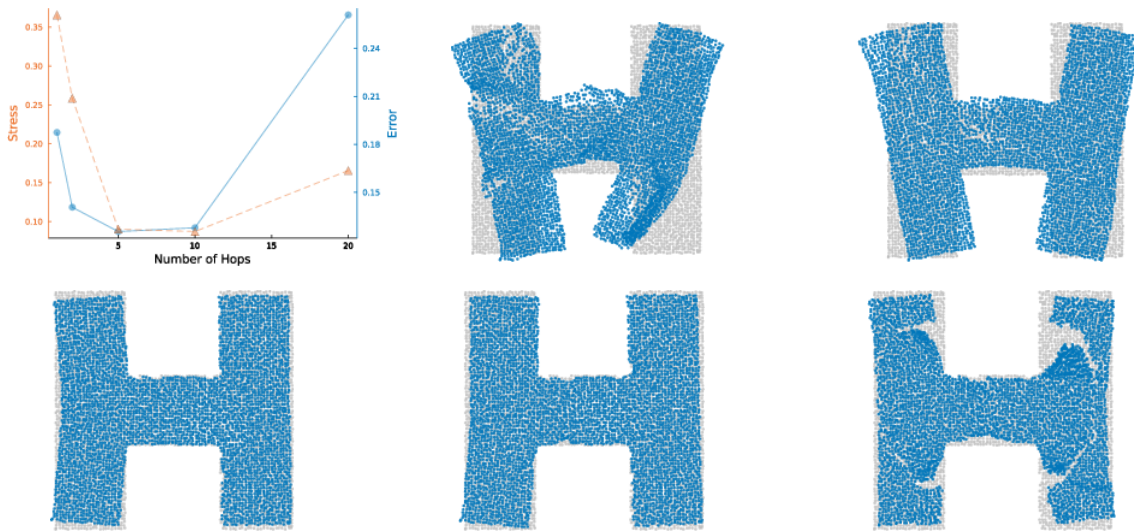


Figure 4.4: Experiment with  $n = 4278$  points on an H-shaped domain or ‘dumbbell’ with  $\sigma = 0.15$ . Top left: Comparison between stress and embedding error. In reading order, the remaining plots show the output of MDS-MAP(P) with number of hops  $h = 1, 2, 5, 10, 20$ .

Euclidean unless the domain is convex. The choice of a smaller patch size enables MDS-MAP(P) to better avoid that bias, as it only relies on being able to cover the domain with approximately convex balls the size of the patches. Thus the number of hops can be understood as controlling model complexity here: the smaller the number of hops, the smaller the patch size, and the more flexible and therefore complex the domain shape model being implicitly fitted. However, in the presence of noise, one also has to contend with the variance, as the smaller a patch is, the more difficult it may be to accurately embed it — although the situation is not quite black-and-white in this regard. Tracking the stress is meant to provide a data-driven way to strike a good compromise

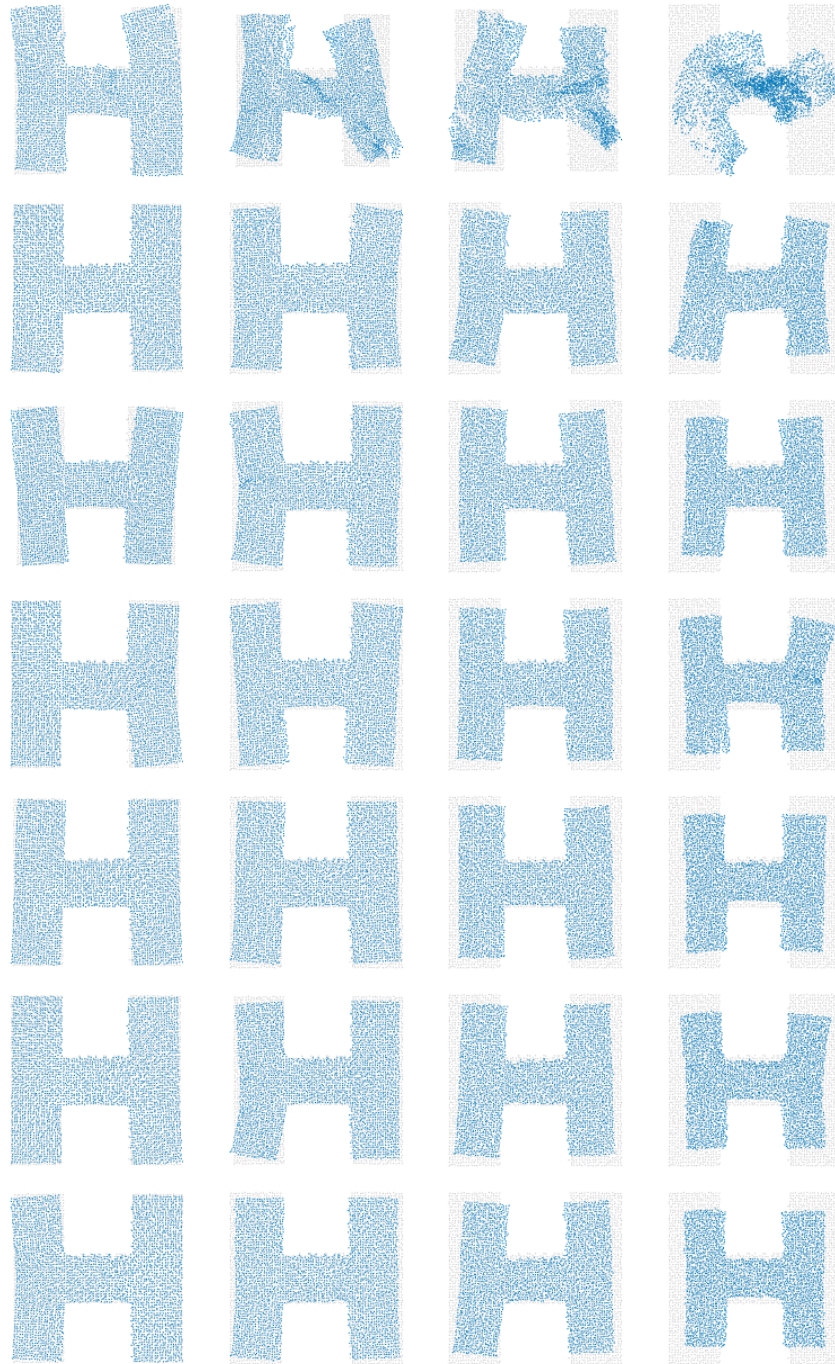


Figure 4.5: In this experiment, we look at the effect of noise on the optimal parameter choice. The dataset features  $n = 2866$  points on an H-shaped domain. Figures in the  $i$ th column have noise  $\sigma = 0.1i$  and the  $j$ th row uses number of hops =  $j$ , for  $i \in [4], j \in [7]$ . Note that, as the noise increases, the embeddings tend to shrink. The shrinkage appears to be caused by the under-approximation of distances in the shortest path estimation step of the algorithm.

between the bias and variance just discussed.

## 4.2 Intercity distances

Beyond synthetic datasets, we also examined the application of our approach to the problem of locating cities in a geographical region (California and Texas) using intercity distances. The latitude and longitude of each city are readily available online<sup>2</sup>. The Haversine formula is used to construct the observed dissimilarity matrix of as-the-crow-flies distances from the geographical coordinates. That is, if  $(\lambda_1, \varphi_1), (\lambda_2, \varphi_2)$  denote the latitude and longitude of a pair of cities, then their distance is computed as follows

$$2 \arcsin \sqrt{\sin^2(\frac{1}{2}(\varphi_2 - \varphi_1)) + \cos(\varphi_1) \cos(\varphi_2) \sin^2(\frac{1}{2}(\lambda_2 - \lambda_1))} .$$

We work with the  $k = 12$  nearest neighbor graph. Although no noise is added, we note that even without noise an exact realization in the plane is not possible since the points are effectively on a curved surface (the surface of the Earth). Figure 4.6 displays the result of applying MDS-MAP(P) to the intercity distances of California. To illustrate the size of patches for the different choices of number of hops, cities that are in a patch surrounding the capital Sacramento are highlighted. Figure 4.7 shows the results for Texas with the patch of the capital Austin being highlighted.

## 5 Dimensionality reduction

Dimensionality reduction (DR) is the problem of embedding points in a possibly high-dimensional Euclidean space into a lower-dimensional Euclidean space while preserving some information pertaining to the data as much as possible. More specifically, we consider the setting where the intrinsic distance information is what needs to be preserved. Note that, unlike (metric) MDS where the data are a set of pairwise dissimilarities, the data in DR are in the form of a point set.

### 5.1 Manifold learning problem

When the points are believed to be on or near a smooth surface, DR is sometimes known as *manifold learning*. Given a set of points  $z_1, \dots, z_n \in \mathbb{R}^{p_0}$ , believed to be sampled from a smooth surface or manifold  $\mathcal{M}$  of dimension  $p < p_0$ , the goal is to embed these points in  $\mathbb{R}^p$  in such a way as to preserve the intrinsic pairwise distances as much as possible. For  $z, z' \in \mathcal{M}$ , their intrinsic distance on  $\mathcal{M}$  is defined as the length of the shortest path on  $\mathcal{M}$  connecting  $z$  and  $z'$ , which we denote  $d_{\mathcal{M}}(z, z')$ . The goal then is to find  $y_1, \dots, y_n \in \mathbb{R}^p$  such that  $\|y_i - y_j\| \approx d_{\mathcal{M}}(z_i, z_j)$  for all or most  $i < j$ .

The realizable case here corresponds to the situation where it is possible to have equality, which practically means that the underlying supporting surface  $\mathcal{M}$  is isometric to a domain of  $\mathbb{R}^p$ . In that case, there is  $x_1, \dots, x_n \in \Omega \subset \mathbb{R}^p$  and an isometry  $\varphi : \Omega \rightarrow \mathcal{M}$  such that  $z_i = \varphi(x_i)$  for all  $i$ . The goal, then, is to recover the configuration  $x_1, \dots, x_n$  — up to a rigid transformation, necessarily.

### 5.2 Methods

The earliest method for DR is principal component analysis (PCA), which also remains the most popular to this day. While, as is well-known, PCA provides the best embedding (in the desired

---

<sup>2</sup>For example, at <https://simplemaps.com/data/us-cities>

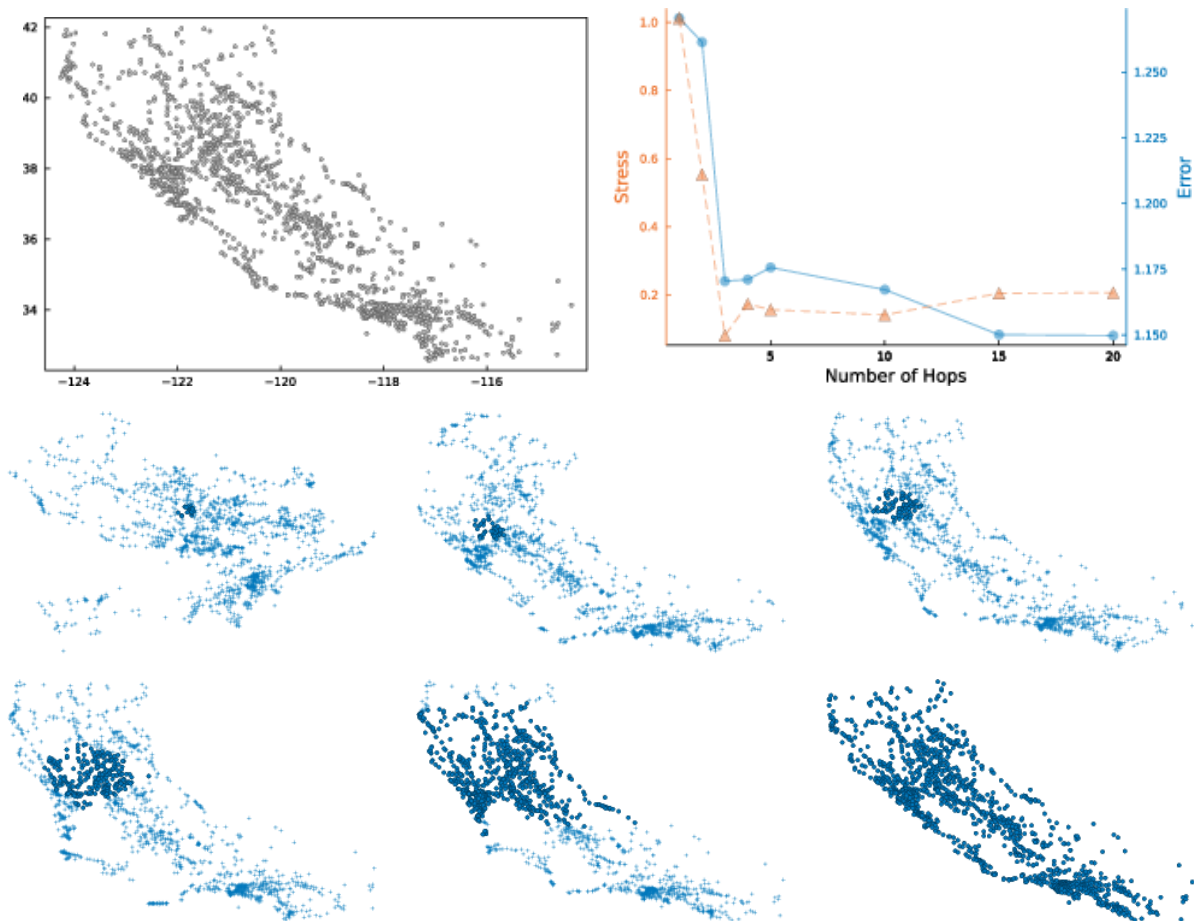


Figure 4.6: MDS-MAP(P) applied to the California intercity dataset. Top left: Plot of cities in California using ground truth latitude and longitude. Top right: Comparison between stress and embedding error. Bottom: In reading order, output of MDS-MAP(P) with number of hops  $h = 1, 2, 3, 5, 10, 20$ . In each case, the patch originating in Sacramento is highlighted.

dimension, still denoted  $p$ ) among linear maps, it can perform poorly when the points lie on or near a curved surface, and this deficiency has motivated the introduction of many other methods for DR.

We will not review the extensive literature that has resulted, but rather focus on the strong parallel between DR and MDS. We start with the well-known relationship between PCA and classical scaling (CS). The two methods are sometimes confused even though they address different problems: Indeed, it turns out that they coincide when CS is applied to the pairwise distances between the data points. In fact, any method for MDS can be turned into a method for DR in exactly the same way: Apply the MDS method to the pairwise distances between the data points. We do so with MDS-MAP(P) to showcase our approach to tuning parameter selection in the context of DR.

When the points are believed to be on or near a smooth surface — the *manifold learning* setting — its intrinsic distance metric is close to the ambient Euclidean metric, but only locally. This thinking is at the core of *isometric feature mapping (Isomap)* [59, 62], and although this was not known to the authors, Isomap consists in applying MDS-D [37] to the local distances. Map-stitching such as local linear embedding [47], manifold charting [13], diffusion maps [16], Hessian

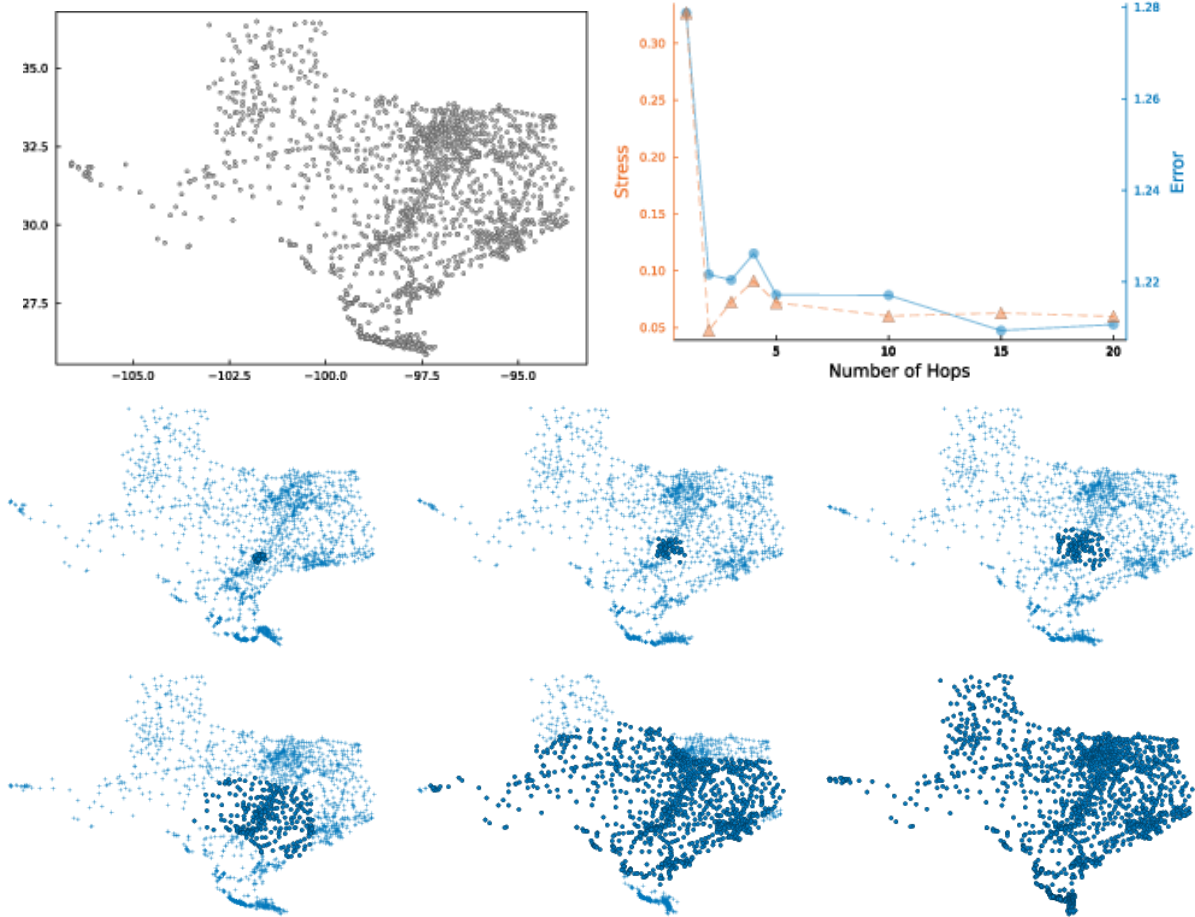


Figure 4.7: MDS-MAP(P) applied to the Texas intercity dataset. Top left: Plot of cities in Texas using ground truth latitude and longitude. Top right: Comparison between stress and embedding error. Bottom: In reading order, output of MDS-MAP(P) with number of hops  $h = 1, 2, 3, 5, 10, 20$ . In each case, the patch originating in Austin is highlighted.

eigenmaps [23], and local tangent space alignment [72], are very similar to patch-stitching methods in MDS already mentioned [19, 24, 35, 38, 53, 60, 71]. The Laplacian eigenmaps of Belkin and Niyogi [9] are closely related to the spectral graph drawing method of Koren [34]. Maximum variance unfolding [68] was concurrently suggested by some of the same authors as a method for sensor network localization [69].

This parallel has been known for quite some time, at least by some, including Chen and Buja [14], who draw inspiration from the extensive literature on graph drawing, and in particular, force-directed methods, to suggest their Local MDS algorithm. See also [46, 52], where the same general idea is manifest.

**Local Isomap** We leverage this parallel between DR and MDS to port our approach to tuning parameter selection to the setting of DR. We continue to use MDS-MAP(P) as an emblematic example. When turned into a method for DR, it resembles a form of *local Isomap*, which we describe in Algorithm 4.

Isomap — which is the equivalent of MDS-MAP [54] — is known to work well in the realizable case when the underlying surface is isometric to a convex domain of the embedding space. (We have

---

**Algorithm 4:** Local Isomap via MDS-MAP(P)
 

---

**Data:** Data points  $z_1, \dots, z_n \in \mathbb{R}^{p_0}$ , connectivity radius  $r$ , embedding dimension  $p$

**Result:** Configuration  $y_1, \dots, y_n \in \mathbb{R}^p$

- 1 Form the neighborhood graph on  $x_1, \dots, x_n$  with connectivity radius  $r$ ;
  - 2 Apply MDS-MAP(P) to the resulting weighted graph to obtain an embedding  $y_1, \dots, y_n$ ;
- 

recently shown that Isomap is not minimax optimal, but can be made so by a sharper estimation of the intrinsic distances [3].) We are therefore able to anticipate that local Isomap — which is the equivalent of MDS-MAP [53] — will perform well in the realizable case, even when the reference domain is non-convex. This is largely borne out in our experiments.

### 5.3 Parameter tuning by stress minimization

Assuming, as we have done, that the embedding dimension  $p$  is given, local Isomap relies on two tuning parameters: the connectivity radius  $r$  in Step 1 and the number of hops  $h$  required by MDS-MAP(P) in Step 2.

While we continue to advocate that the number of hops be chosen by minimization of the stress, the connectivity radius cannot be chosen in the same way: Indeed, the connectivity radius is what defines the graph, which in turn defines the stress as in (2.3).

Many methods in manifold learning rely on a construction of a neighborhood graph and our understanding is that the choice of connectivity radius remains ad hoc. In our experiments, we follow standard practice and choose as  $r$  a small multiple of that is needed for the resulting graph to be connected.

### 5.4 Experiments

Although it is easy to anticipate that local Isomap will behave in the context of DR in a way that is parallel to how MDS-MAP(P) behaves in the context of MDS, we perform some simple numerical experiments to confirm this. We focus on the realizable case.

To simulate the data in the manifold learning setting, we start with data points in  $\mathbb{R}^2$  as in Section 4, and then embed these into  $\mathbb{R}^3$ . We chose to work with the hollow rectangle of Figure 4.2. Note that here, unlike in the MDS setting of Section 4, the graph structure is not given but is chosen in Step 1 of local Isomap. We used two different embeddings that seem popular in the literature: a cylindrical surface based on an S curve and a cylindrical surface based on a spiral, often referred to as a Swiss roll. The ‘S’ surface is obtained via the following embedding of  $[0, 1]^2$ ,

$$\varphi_{S,\alpha}(u, v) = (\alpha^{-1} \sin(\alpha v), u, \text{sign}(\alpha v) \alpha^{-1} (\cos(\alpha v) - 1)), \quad (5.1)$$

while the Swiss roll is obtained via

$$\varphi_{\text{Swiss},\alpha}(u, v) = (s(u, v) \cos(\alpha s(u, v)), u, s(u, v) \sin(\alpha s(u, v))), \quad (5.2)$$

where  $s(u, v)$  is the solution to  $\int_0^s \sqrt{1 + (\alpha t)^2} dt = v$ . The parameter  $\alpha$  allows us to increase the curvature of the resulting surface. (In our experiments,  $\alpha = 10$  for the ‘S’ surface and  $= 50$  for the Swiss roll.) Although the estimation of the local intrinsic distances by the ambient Euclidean distances implies a bias which already plays the role of noise, we add a small amount of Gaussian noise to obtain the data points: see Figure 5.1 for the ‘S’ surface and Figure 5.2 for the Swiss roll.

The embeddings produced by local Isomap for various choice of the number of hops are displayed in Figure 5.3 for the ‘S’ surface and Figure 5.4 for the Swiss roll.

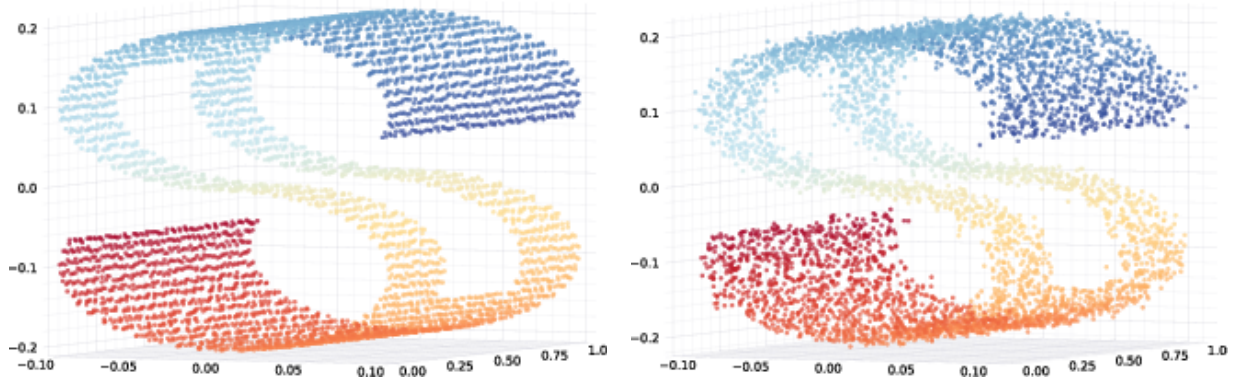


Figure 5.1: Data points (about  $n \approx 4000$  of them) generated based on embedding the hollow rectangle of Figure 4.2 as an ‘S’ surface using (5.1), without (left) and with (right) added noise.

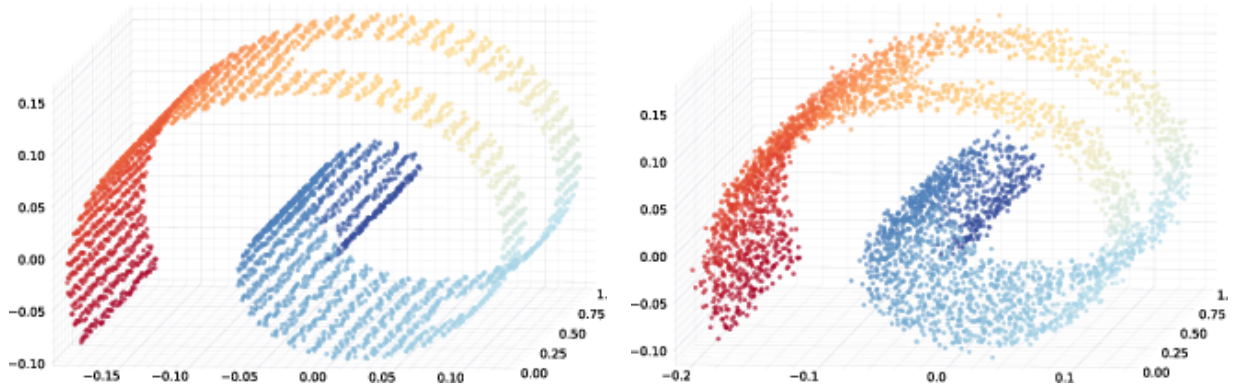


Figure 5.2: Data points (about  $n \approx 4000$  of them) generated based on embedding the hollow rectangle of Figure 4.2 as a Swiss roll using (5.2), without (left) and with (right) added noise.

## 6 Discussion

### 6.1 Choice of embedding dimension

Some applications, as in sensor network localization where the items are known to be in a 2D physical space, the embedding dimension comes with the problem itself. In other situations, it needs to be chosen by the analyst. This is discussed in [12, Sec 3.5], where the suggested approach consists, for a particular method under consideration, in plotting the stress for the output embedding as a function of the embedding dimension, and look for an ‘elbow’ in the resulting plot indicating that the gains in stress from increasing the dimension have started to dampen.

While this ad hoc approach can be formalized for particular methods such as classical scaling, we can already see that the situation is very different here as compared to choosing a tuning parameter such as the number of hops for MDS-MAP(P): Indeed, the stress is decreasing as a function of the embedding dimension and thus cannot be used to select the dimension. But once the embedding dimension is chosen — one way or another — the stress may be fruitfully used to select any other parameter.

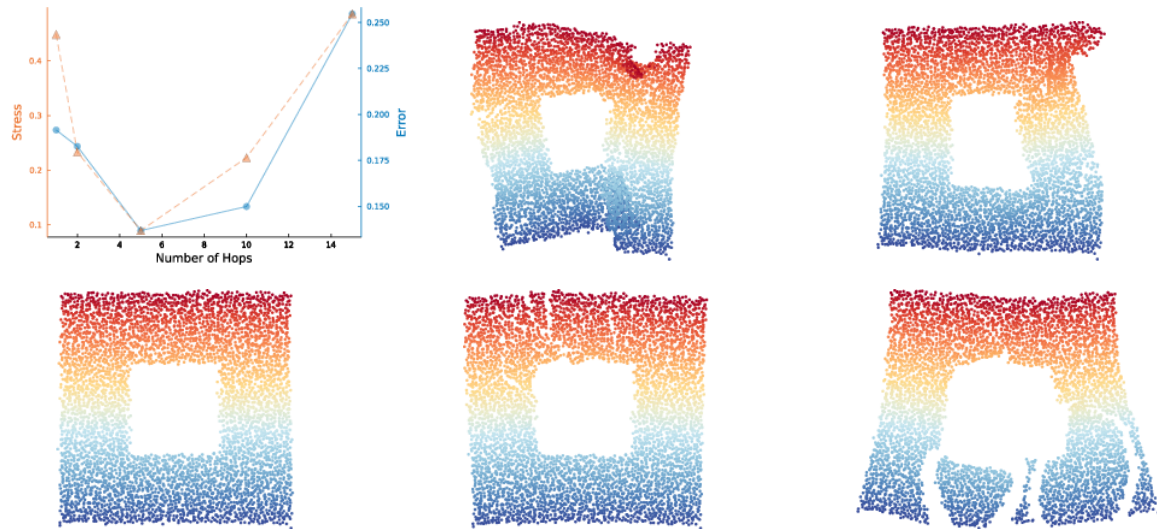


Figure 5.3: Experiment with  $n = 5008$  points near an ‘S’ surface. Top left: Comparison between stress and embedding error. In reading order, the remaining plots show the output of local Isomap with number of hops  $h = 1, 2, 5, 10, 15$ .

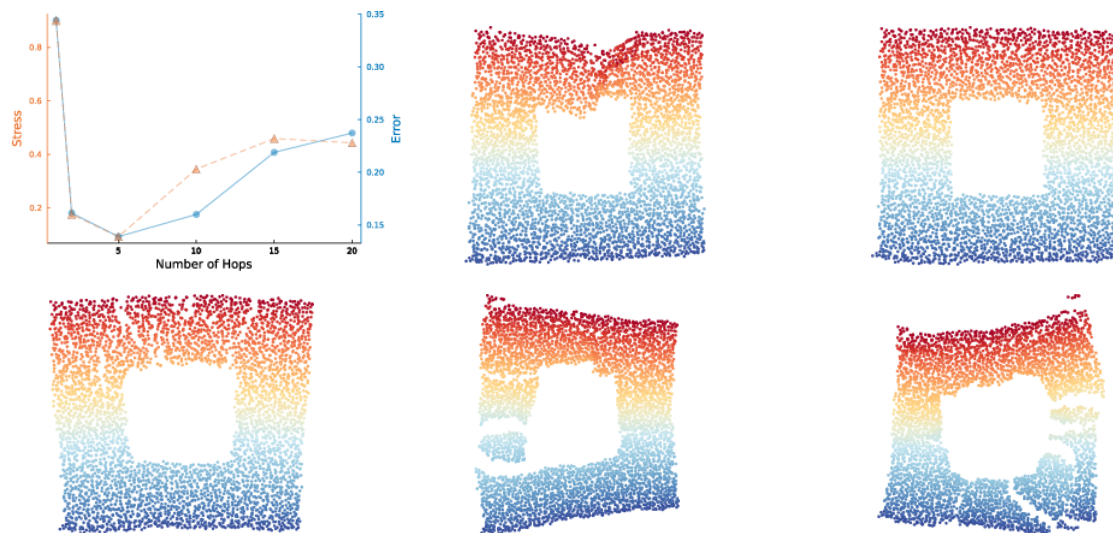


Figure 5.4: Experiment with  $n = 4137$  points near a Swiss roll. Top left: Comparison between stress and embedding error. In reading order, the remaining plots show the output of local Isomap with number of hops  $h = 2, 5, 10, 15, 20$ .

## 6.2 Non-metric MDS

While our discussion has entirely focused on the *metric* variant of MDS, equally important is the *non-metric* (aka *ordinal*) variant in which only ordinal information on the pairwise dissimilarities is available [12, Ch 9]. The non-metric setting was considered early on as it has arguably more applications in psychometrics than the metric setting. Pioneering work includes that of Kruskal [36] and Shepard [56, 57, 58]. See [33, 40] for some historical background.

In non-metric MDS, what is available to the analyst are  $\xi_{ijkl}$  for some  $(i, j, k, l) \in \mathcal{E} \subset [n]^4$ , where  $\xi_{ijkl} := \mathbb{I}\{d_{ij} < d_{kl}\}$ . The goal is then to produce  $y_1, \dots, y_n \in \mathbb{R}^p$  (where  $p$  is assumed given as

before) such that the  $\zeta_{ijkl} := \mathbb{I}\{\|y_i - y_j\| < \|y_k - y_l\|\}$  agree as much as possible with the  $\xi_{ijkl}$ .

Patch-stitching seems uncommon in the non-metric setting. We are only aware of [20], where it is used in the related problem of embedding a nearest-neighbor graph. Ordinal embedding is leveraged in a metric context in [66] to allow for additional flexibility. Regardless, it is straightforward to adapt patch-stitching to the non-metric setting: simply embed the patches using a method for non-metric MDS and then stitch the resulting patches as usual. The number of hops defining the patch size would also need to be chosen and a non-metric equivalent of the stress can be used for that purpose. A natural option is to use the number of disagreements between the data dissimilarity comparisons and the corresponding embedded distance comparisons

$$\sum_{(i,j,k,l) \in \mathcal{E}} \mathbb{I}\{\zeta_{ijkl} \neq \xi_{ijkl}\}. \quad (6.1)$$

We are currently exploring this in a larger context and will report on that elsewhere.

We note that, once again, the embedding dimension is not like any other tuning parameter. In particular, the non-metric stress defined in (6.1) does not seem to be useful for selecting the dimension. For example, when all comparisons are available, meaning when  $\xi_{ijkl}$  is available for all  $(i, j, k, l) \in [n]^4$ , it is always possible to obtain an embedding in dimension  $n - 1$  with zero stress. Indeed, it is known since the work of Torgerson [64] that, for any dissimilarities  $(d_{ij})$ , where  $d_{ii} = 0$  and  $d_{ij} = d_{ji} \geq 0$ , it is always possible to find a constant  $c$  such that  $(d_{ij} + c)$  is Euclidean in dimension  $n - 1$ . Now, the setting where all comparisons are available is equivalent to the setting where the analyst is provided with a complete ranking of the dissimilarities:  $(r_{ij} : i < j)$ , where  $r_{ij}$  is the rank in increasing order of  $d_{ij}$  among the dissimilarities  $\{d_{kl} : k < l\}$ . Letting  $(r_{ij})$ , with  $r_{ii} = 0$  and  $r_{ji} = r_{ij}$ , play the role of dissimilarities, there is a constant  $c$  such that a perfect embedding of  $(r_{ij} + c)$  exists in dimension  $n - 1$ . Then such an embedding has zero non-metric stress, since the ordering in  $(r_{ij} + c)$  is the same as in  $(r_{ij})$ .

## References

- [1] Anderson, B. D., I. Shames, G. Mao, and B. Fidan (2010). Formal theory of noisy sensor network localization. *SIAM Journal on Discrete Mathematics* 24(2), 684–698.
- [2] Arias-Castro, E., A. Channarond, B. Pelletier, and N. Verzelen (2021). On the estimation of latent distances using graph distances. *Electronic Journal of Statistics* 15(1), 722–747.
- [3] Arias-Castro, E. and P. A. Chau (2020). Minimax estimation of distances on a surface and minimax manifold learning in the isometric-to-convex setting. *arXiv preprint arXiv:2011.12478*.
- [4] Arias-Castro, E., A. Javanmard, and B. Pelletier (2020). Perturbation bounds for procrustes, classical scaling, and trilateration, with applications to manifold learning. *Journal of Machine Learning Research* 21, 1–37.
- [5] Arias-Castro, E. and T. Le Gouic (2019). Unconstrained and curvature-constrained shortest-path distances and their approximation. *Discrete & Computational Geometry* 62(1), 1–28.
- [6] Asimow, L. and B. Roth (1978). The rigidity of graphs. *Transactions of the American Mathematical Society* 245, 279–289.
- [7] Aspnes, J., T. Eren, D. Goldenberg, A. Morse, W. Whiteley, Y. Yang, B. Anderson, and P. Belhumeur (2006). A theory of network localization. *IEEE Transactions on Mobile Computing* 5(12), 1663–1678.
- [8] Aspnes, J., D. Goldenberg, and Y. R. Yang (2004). On the computational complexity of sensor network localization. In *International Symposium on Algorithms and Experiments for Sensor Systems, Wireless Networks and Distributed Robotics*, pp. 32–44.

- [9] Belkin, M. and P. Niyogi (2003). Laplacian eigenmaps for dimensionality reduction and data representation. *Neural Computation* 15(16), 1373–1396.
- [10] Bernstein, M., V. De Silva, J. Langford, and J. Tenenbaum (2000). Graph approximations to geodesics on embedded manifolds. Technical report, Department of Psychology, Stanford University.
- [11] Biswas, P., T.-C. Liang, K.-C. Toh, Y. Ye, and T.-C. Wang (2006). Semidefinite programming approaches for sensor network localization with noisy distance measurements. *IEEE Transactions on Automation Science and Engineering* 3(4), 360–371.
- [12] Borg, I. and P. J. Groenen (2005). *Modern Multidimensional Scaling: Theory and Applications*. Springer Science & Business Media.
- [13] Brand, M. (2003). Charting a manifold. *Advances in Neural Information Processing Systems*, 985–992.
- [14] Chen, L. and A. Buja (2009). Local multidimensional scaling for nonlinear dimension reduction, graph drawing, and proximity analysis. *Journal of the American Statistical Association* 104(485), 209–219.
- [15] Chowdhury, T. J., C. Elkin, V. Devabhaktuni, D. B. Rawat, and J. Oluoch (2016). Advances on localization techniques for wireless sensor networks: A survey. *Computer Networks* 110, 284–305.
- [16] Coifman, R. and S. Lafon (2006). Diffusion maps. *Applied and Computational Harmonic Analysis* 21(1), 5–30.
- [17] Connelly, R. (2005). Generic global rigidity. *Discrete & Computational Geometry* 33(4), 549–563.
- [18] Costa, J. A., N. Patwari, and A. O. Hero (2006). Distributed weighted-multidimensional scaling for node localization in sensor networks. *ACM Transactions on Sensor Networks* 2(1), 39–64.
- [19] Cucuringu, M., Y. Lipman, and A. Singer (2012). Sensor network localization by eigenvector synchronization over the Euclidean group. *ACM Transactions on Sensor Networks (TOSN)* 8(3), 19.
- [20] Cucuringu, M. and J. Woodworth (2015). Ordinal embedding of unweighted kNN graphs via synchronization. In *IEEE International Workshop on Machine Learning for Signal Processing*, pp. 1–6.
- [21] de Leeuw, J. and P. Mair (2009). Multidimensional scaling using majorization: SMACOF in R. *Journal of Statistical Software, Articles* 31(3), 1–30.
- [22] de Silva, V. and J. B. Tenenbaum (2004). Sparse multidimensional scaling using landmark points. Technical report, Stanford University.
- [23] Donoho, D. and C. Grimes (2003). Hessian eigenmaps: Locally linear embedding techniques for high-dimensional data. *Proceedings of the National Academy of Sciences* 100(10), 5591–5596.
- [24] Drusvyatskiy, D., N. Krislock, Y.-L. Voronin, and H. Wolkowicz (2017). Noisy Euclidean distance realization: Robust facial reduction and the Pareto frontier. *SIAM Journal on Optimization* 27(4), 2301–2331.
- [25] Elad, A. and R. Kimmel (2003). On bending invariant signatures for surfaces. *IEEE Transactions on Pattern Analysis and Machine Intelligence* 25(10), 1285–1295.
- [26] Eren, T., O. Goldenberg, W. Whiteley, Y. R. Yang, A. S. Morse, B. D. Anderson, and P. N. Belhumeur (2004). Rigidity, computation, and randomization in network localization. In *Conference of the IEEE Computer and Communications Societies (INFOCOM)*, Volume 4, pp. 2673–2684.
- [27] Fang, J., M. Cao, A. S. Morse, and B. D. Anderson (2009). Sequential localization of sensor networks. *SIAM Journal on Control and Optimization* 48(1), 321–350.
- [28] Floyd, R. W. (1962). Algorithm 97: Shortest path. *Communications of the ACM* 5(6), 345.

- [29] Gower, J. C. (1966). Some distance properties of latent root and vector methods used in multivariate analysis. *Biometrika* 53(3-4), 325–338.
- [30] Hastie, T., R. Tibshirani, and J. Friedman (2009). *The Elements of Statistical Learning: Data Mining, Inference, and Prediction* (2nd ed.). Springer Science & Business Media.
- [31] Jackson, B. and T. Jordán (2005). Connected rigidity matroids and unique realizations of graphs. *Journal of Combinatorial Theory, Series B* 94(1), 1–29.
- [32] Javanmard, A. and A. Montanari (2013). Localization from incomplete noisy distance measurements. *Foundations of Computational Mathematics* 13(3), 297–345.
- [33] Jaworska, N. and A. Chupetlovska-Anastasova (2009). A review of multidimensional scaling (MDS) and its utility in various psychological domains. *Tutorials in Quantitative Methods for Psychology* 5(1), 1–10.
- [34] Koren, Y. (2003). On spectral graph drawing. In *International Computing and Combinatorics Conference*, pp. 496–508.
- [35] Koren, Y., C. Gotsman, and M. Ben-Chen (2005). PATCHWORK: Efficient localization for sensor networks by distributed global optimization. Technical report.
- [36] Kruskal, J. B. (1964). Multidimensional scaling by optimizing goodness of fit to a nonmetric hypothesis. *Psychometrika* 29, 1–27.
- [37] Kruskal, J. B. and J. B. Seery (1980). Designing network diagrams. In *Conference on Social Graphics*, pp. 22–50.
- [38] Kwon, O.-H. and H.-J. Song (2007). Localization through map stitching in wireless sensor networks. *IEEE Transactions on Parallel and Distributed Systems* 19(1), 93–105.
- [39] Laman, G. (1970). On graphs and rigidity of plane skeletal structures. *Journal of Engineering Mathematics* 4(4), 331–340.
- [40] Mead, A. (1992). Review of the development of multidimensional scaling methods. *Journal of the Royal Statistical Society: Series D (The Statistician)* 41(1), 27–39.
- [41] Moore, D., J. Leonard, D. Rus, and S. Teller (2004). Robust distributed network localization with noisy range measurements. In *ACM Conference on Embedded Networked Sensor Systems*, pp. 50–61.
- [42] Oh, S., A. Montanari, and A. Karbasi (2010). Sensor network localization from local connectivity: Performance analysis for the MDS-map algorithm. In *IEEE Information Theory Workshop on Information Theory*, pp. 1–5.
- [43] Pearson, K. (1901). LIII. On lines and planes of closest fit to systems of points in space. *The London, Edinburgh, and Dublin Philosophical Magazine and Journal of Science* 2(11), 559–572.
- [44] Penrose, M. (2003). *Random Geometric Graphs*. Oxford University Press.
- [45] Pettie, S. and V. Ramachandran (2002). Computing shortest paths with comparisons and additions. In *ACM-SIAM Symposium on Discrete Algorithms*, pp. 267–276.
- [46] Rosman, G., M. M. Bronstein, A. M. Bronstein, and R. Kimmel (2010). Nonlinear dimensionality reduction by topologically constrained isometric embedding. *International Journal of Computer Vision* 89(1), 56–68.
- [47] Roweis, S. and L. Saul (2000). Nonlinear dimensionality reduction by locally linear embedding. *Science* 290(5500), 2323–2326.
- [48] Sao, P., R. Kannan, P. Gera, and R. Vuduc (2020). A supernodal all-pairs shortest path algorithm. In *ACM Symposium on Principles and Practice of Parallel Programming*, pp. 250–261.
- [49] Savarese, C., J. Rabaey, and J. Beutel (2001). Location in distributed ad-hoc wireless sensor networks. In *IEEE International Conference on Acoustics, Speech, and Signal Processing*, Volume 4, pp. 2037–2040 vol.4.
- [50] Schoenberg, I. J. (1935). Remarks to Maurice Fréchet’s article “Sur la definition axiomatique

- d'une classe d'espace distances vectoriellement applicable sur l'espace de Hilbert. *Annals of Mathematics*, 724–732.
- [51] Schönemann, P. H. (1966). A generalized solution of the orthogonal procrustes problem. *Psychometrika* 31(1), 1–10.
- [52] Schwartz, A. and R. Talmon (2019). Intrinsic isometric manifold learning with application to localization. *SIAM Journal on Imaging Sciences* 12(3), 1347–1391.
- [53] Shang, Y. and W. Ruml (2004). Improved MDS-based localization. In *Conference of the IEEE Computer and Communications Societies*, Volume 4, pp. 2640–2651.
- [54] Shang, Y., W. Ruml, Y. Zhang, and M. P. Fromherz (2003). Localization from mere connectivity. In *ACM International Symposium on Mobile Ad Hoc Networking and Computing*, pp. 201–212.
- [55] Shang, Y., H. Shi, and A. Ahmed (2004). Performance study of localization methods for ad-hoc sensor networks. In *IEEE International Conference on Mobile Ad-hoc and Sensor Systems*.
- [56] Shepard, R. N. (1962a). The analysis of proximities: multidimensional scaling with an unknown distance function. I. *Psychometrika* 27, 125–140.
- [57] Shepard, R. N. (1962b). The analysis of proximities: multidimensional scaling with an unknown distance function. II. *Psychometrika* 27, 219–246.
- [58] Shepard, R. N. (1966). Metric structures in ordinal data. *Journal of Mathematical Psychology* 3(2), 287–315.
- [59] Silva, V. and J. Tenenbaum (2002). Global versus local methods in nonlinear dimensionality reduction. *Advances in Neural Information Processing Systems* 15, 705–712.
- [60] Singer, A. (2008). A remark on global positioning from local distances. *Proceedings of the National Academy of Sciences* 105(28), 9507–9511.
- [61] So, A. M.-C. and Y. Ye (2007). Theory of semidefinite programming for sensor network localization. *Mathematical Programming* 109(2-3), 367–384.
- [62] Tenenbaum, J. B., V. d. Silva, and J. C. Langford (2000). A global geometric framework for nonlinear dimensionality reduction. *Science* 290(5500), 2319–2323.
- [63] Thorpe, M. F. and P. M. Duxbury (1999). *Rigidity Theory and Applications*. Springer Science & Business Media.
- [64] Torgerson, W. S. (1952). Multidimensional scaling: I. theory and methods of scaling. *Psychometrika* 17(4), 401–419.
- [65] Torgerson, W. S. (1958). *Theory and Methods of Scaling*. Wiley.
- [66] Vivekanandan, V. and V. W. Wong (2006). Ordinal MDS-based localization for wireless sensor networks. In *IEEE Vehicular Technology Conference*, pp. 1–5.
- [67] Wang, Q. and K. L. Boyer (2013). Feature learning by multidimensional scaling and its applications in object recognition. In *IEEE Conference on Graphics, Patterns and Images*, pp. 8–15.
- [68] Weinberger, K., F. Sha, and L. Saul (2004). Learning a kernel matrix for nonlinear dimensionality reduction. In *International Conference on Machine Learning*, pp. 106.
- [69] Weinberger, K. Q., F. Sha, Q. Zhu, and L. K. Saul (2006). Graph laplacian regularization for large-scale semidefinite programming. In *Advances in Neural Information Processing Systems*, pp. 1489–1496.
- [70] Yang, T., J. Liu, L. McMillan, and W. Wang (2006). A fast approximation to multidimensional scaling. In *IEEE Workshop on Computational Intensive Methods for Computer Vision*.
- [71] Zhang, L., L. Liu, C. Gotsman, and S. J. Gortler (2010). An as-rigid-as-possible approach to sensor network localization. *ACM Transactions on Sensor Networks* 6(4), 35.
- [72] Zhang, Z. and H. Zha (2004). Principal manifolds and nonlinear dimension reduction via tangent space alignment. *SIAM Journal on Scientific Computing* 26(1), 313–338.